$SrSnO_3$ Nanostructures: Synthesis, Characterization, and Photocatalytic Properties

Di Chen and Jinhua Ye*

Photocatalytic Materials Center, National Institute for Materials Science (NIMS), 1-2-1 Sengen, Tsukuba, Ibaraki 305-0047, Japan

Received May 15, 2007. Revised Manuscript Received July 12, 2007

Dumbbell-like and rodlike nanostructures of $SrSnO_3$ were successfully synthesized by calcination of the corresponding hydrothermally prepared precursors, $SrSn(OH)_6$, at 1100 °C in air. The structure and morphology of the as-synthesized sample were characterized by X-ray diffraction, scanning electron microscopy, transmission electron microscopy, ultraviolet−visible diffuse reflectance spectroscopy, and volumetric adsorption method (BET). The photocatalytic activity of the $SrSnO_3$ products for the H_2 and O_2 evolution was systematically investigated under UV light irradiation. It was found that nanostructured $SrSnO_3$ photocatalysts with different morphologies possess 10 times more photoactivity than the solid-state reaction sample under UV light irradiation.

1. Introduction

Since the Honda-Fujishima effect was reported using a TiO_2 semiconductor electrode, water splitting into H_2 and O_2 with semiconductor photocatalysts has been studied for a long time in the fields of catalysis, electrochemistry, photochemistry, and organic and inorganic chemistry.[1] Although much work has been devoted to exploit new photocatalysts responsive to UV and visible light irradiation, the number of effective photocatalysts that were able to decompose water into H_2 and O_2 is quite limited.[2−8] Therefore, it is still very important to develop a new type of photocatalysts with high photoactivity.

Direct synthesis of inorganic materials with specific morphology and orientation via simple route has attracted intensive interest in material science.[9−13] Usually, the choice of initial materials or the manner in which they organize greatly affected the product's novel optical and electronic properties. Thus, these results offered new opportunities for investigating product's size- and shape-dependent physical and chemical properties, which are extremely important to industrial application.[14,15]

Hydrothermal synthesis as a well-known traditional wet chemical process is promising for the direct preparation of advanced nanostructures because of its advantages.[16] It is believed that this method generates highly crystalline products with high purity, narrow size distribution, and low aggregation. Moreover, the morphology and crystal form of the products can also be controlled by adjusting the hydrothermal reaction conditions. Recently, this facile wet chemical route has been widely employed to prepare nanosized crystallites with high purity and novel morphologies to enhance photocatalytic activity. For example, rodlike $ZnWO_4$ showed better activity for the degradation of formaldehyde than TiO_2 (P-25) under UV light irradiation;[17] nanosized Bi_2WO_6 sheets exhibited relatively high photochemical activity for the decomposition of rhodamine-B under visible light irradiation ($\lambda > 420$ nm);[18] fibrous $SrTiO_3$ particles showed better performance in the destruction of nitrogen monoxide in near-ultraviolet light range;[19] octrahedral Cu_2O nanoparticles possessed much higher adsorption ability and photoactivity than cubic sample under visible light region;[20] and well-crystallized $BiVO_4$ powders showed high photocatalytic activity for O_2 evolution from an aqueous $AgNO_3$ solution under visible-light irradiation, and it is interesting that $BiVO_4$ with various morphologies showed different photoactivity at experimental conditions.[21] All these results may suggest that it is possible to synthesize photocatalysts with unique morphologies by this simple and efficient method.

* To whom correspondence should be addressed. Fax: +81-29-8592301. E-mail: jinhua.ye@nims.go.jp.

(1) Fujishima, A.; Honda, K. *Nature (London)* **1972**, *238*, 37.
(2) Sayama, K.; Arakawa, H. *J. Photochem. Photobiol., A* **1994**, *77*, 243.
(3) Domen, K.; Kudo, A.; Onishi, T.; Kosugi, N.; Kuroda, H. *J. Phys. Chem.* **1986**, *90*, 292.
(4) Takata, T.; Furumi, Y.; Shinohara, K.; Tanaka, A.; Hara, M.; Kondo, J. N.; Domen, K. *Chem. Mater.* **1997**, *9*, 1063.
(5) Kato, H.; Kudo, A. *Chem. Phys. Lett.* **1998**, *295*, 487.
(6) Kato, H.; Kudo, A. *Catal. Lett.* **1999**, *58*, 153.
(7) Zou, Z. G.; Ye, J. H.; Sayama, K.; Arakawa, H. *Nature* **2001**, *414*, 625.
(8) Wang, D. F.; Tang, J. W.; Zou, Z. G.; Ye, J. H. *Chem. Mater.* **2005**, *17*, 5177.
(9) Li, M.; Schnablegger, H.; Mann, S. *Nature* **1999**, *402*, 393.
(10) Peng, X. G.; Manna, L.; Yang, W. D.; Wickham, J.; Scher, E.; Kadavanich, A.; Alivisatos, A. P. *Nature* **2000**, *404*, 59.
(11) Whitesides, G. M.; Grzybowski, B. *Science* **2002**, *295*, 2418.
(12) Pileni, M. P. *J. Phys. Chem. B* **2001**, *105*, 3358.
(13) Colfen, H.; Mann, S. *Angew. Chem., Int. Ed.* **2000**, *42*, 2350.
(14) Huang, M. H.; Mao, S.; Feick, H.; Yan, H.; Wu, Y.; Kind, H.; Weber, E.; Russo, R.; Yang, P. *Science* **2001**, *292*, 1897.
(15) Lu, Q.; Gao, F.; Zhao, D. *Chem. Phys. Lett.* **2002**, *360*, 355.
(16) Yu, S. H.; Liu, B.; Mo, M. S.; Huang, J. H.; Liu, X. M.; Qian, Y. T. *Adv. Funct. Mater.* **2003**, *13*, 639.
(17) Fu, H. B.; Lin, J.; Zhang, L. W.; Zhu, Y. F. *Appl. Catal., A* **2006**, *306*, 58.
(18) Fu, H. B.; Pan, C. S.; Yao, W. Q.; Zhu, Y. F. *J. Phys. Chem. B* **2005**, *109*, 22432.
(19) Wang, J. S.; Yin, S.; Sato, T. *Mater. Sci. Eng., B* **2006**, *131*, 248.
(20) Xu, H. L.; Wang, W. Z.; Zhu, W. *J. Phys. Chem. B* **2006**, *110*, 13829.
(21) Yu, J. Q.; Kudo, A. *Adv. Funct. Mater.* **2006**, *16*, 2163.

10.1021/cm071321d CCC: $37.00
Published on Web 08/15/2007

Perovskite type alkaline earth stannates have received considerable attention in recent years as components of ceramic dielectric elements.[22] Strontium stannate, $SrSnO_3$, is a distorted perovskite due to the octahedral tilting distortion driven by a mismatch in the fit of the Sr-site cation to the cuboctahedral cavities in the corner-sharing octahedral network.[23] This material, with a wide band gap, has been reported to be used in humidity sensors.[24] Our group also reported that it exhibited photoactivity for water splitting from aqueous solution under UV light irradiation.[25] In general, strontium stannate is mainly synthesized via the conventional solid-state method, which usually has larger dimension-distribution and needs higher temperature and longer reaction time.[25−27] This might result in the decrease of photocatalytic activity. Herein, we first successfully synthesized $SrSn(OH)_6$ with dumbbell-like and rodlike morphologies via a facile hydrothermal route and then converted the precursors into $SrSnO_3$ with similar nanostructures by calcinations treatment. It is interesting that various $SrSnO_3$ nanostructures show high photoactivity under UV light irradiation. We also found that dissolvable raw reagents used in the present case and the initial stirring treatments have a great effect on the precursor morphology which influences the final morphology and photocatalytic activity of the sample.

2. Experimental Section

Synthesis of $SrSn(OH)_6$ Precursors. The $SrSn(OH)_6$ precursor with different morphologies was synthesized from a simple hydrothermal process. For the synthesis of dumbbell-like precursor, equivalent amounts of $Sr(NO_3)_2$ and Na_2SnO_3 (2 mmol) were dissolved in 15 mL of distilled water, respectively. Then the $Sr(NO_3)_2$ solution was slowly added into the Na_2SnO_3 solution under vigorous magnetic stirring at room temperature (~25 °C). White precipitates were generated promptly. Immediately, the resulting precursor suspension was directly transferred into a Teflon-lined stainless steel autoclave without any pretreatment, which was heated at 180 °C for 16 h. After cooled to room temperature, the product was filtered, washed for several times with distilled water, and then dried in air at 70 °C. The synthesis process of nanorod precursor was similar to that of the dumbbell product except that the mixed $Sr(NO_3)_2$ and Na_2SnO_3 solution was kept magnetic stirring at room temperature (~25 °C) for 2 h before transferring the mixed solution into Teflon-lined stainless steel autoclave.

Synthesis of $SrSnO_3$ Nanostructures. To get the $SrSnO_3$ products, the hydrothermally synthesized precursors with different morphologies were first dried in air and then directly calcined in a furnace at 1100 °C for 6 h in air without any other treatment.

Characterization. The crystal structure of the as-prepared sample was confirmed by the X-ray diffraction pattern (JEOL JDX-3500 Tokyo, Japan). The morphology and size of the sample were characterized by scanning electron microscopy (SEM, JSM-6700F) and by transmission electron microscopy (HRTEM, JEM-3000F) equipped with an X-ray dispersive spectrometer (EDS). UV−vis diffuse reflectance spectra were recorded on a UV/vis spectrometer (UV-2500, Shimadzu) and were converted from reflection to absorbance by the standard Kubelka−Munk method. The surface area was measured on a Gemini 2360 surface area analyzer (Micromeritics, SHIMADZU) by nitrogen absorption at 77 K using the Brunauer−Emmett−Teller (BET) method. The photocatalytic reaction was performed with a closed gas circulation system. An inner irradiation type quartz cell with a 400 W high-pressure Hg lamp was employed. The evolved gas was determined by a thermal conductivity detector (TCD) gas chromatograph (ShimadzuGC-8A), which was connected to the system with a circulating line. The H_2 evolution reaction was performed in CH_3OH/H_2O solution with Pt cocatalyst (catalyst: 0.2 g, Pt: 0.5 wt %, CH_3OH: 50 mL, H_2O: 320 mL), and the O_2 evolution reaction was performed in $AgNO_3$ solution without any cocatalyst (catalyst: 0.2 g, $AgNO_3$: 5 mmol, H_2O: 370 mL). The photonic efficiency or quantum yield of H_2 evolution at $\lambda = 300$ nm was measured by using an interference band-pass filter ($\lambda_0 = 300.0$ nm, Tmax = 20.3%, $\Delta\lambda/2 = 16.7$ nm, Kenko). The light source was a 200 W Hg−Xe lamp, and a thermopile was used for measuring the intensity of incident light and then transferred to the number of incident photons. The apparent quantum yield (%) of H_2 was calculated by the following equation: QY (%) $= N_e/N_p = 2N_{H2}/N_p$, where N_e is the number of reacted electrons, N_{H2} is the number of H_2 molecules evolved, and N_p is the number of incident photons. In all experiments, the photocatalyst particles were suspended in solution by stirring with a magnetic stirrer, and the rotative velocity of the stirrer was set at 500 rpm.

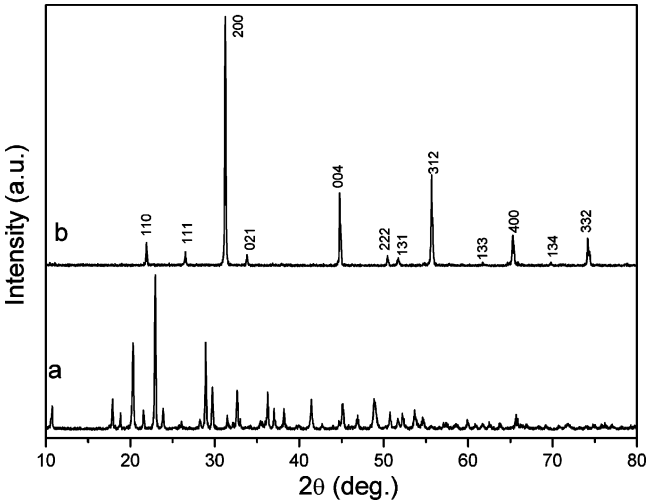

Figure 1. XRD patterns of (a) the precursor $SrSn(OH)_6$ and (b) the $SrSnO_3$ sample obtained from the precursor.

3. Results and Discussion

Structures. Figure 1a shows the XRD pattern of a $SrSn(OH)_6$ precursor obtained from the hydrothermal process. It indicates the formation of pure tetrahedral structure with cell parameters in good agreement with the reported data (JCPDS 09-0086). Figure 1b is the typical XRD pattern of the calcined product. All the peaks in this pattern can be readily indexed to pure orthorhombic perovskite structure $SrSnO_3$ according to the standard card (JCPDS 77-1798). No impurities could be detected in this pattern, which implies the orthorhombic phase $SrSnO_3$ could be obtained from the current synthetic route.

(22) Coffeen, W. W. *J. Am. Ceram. Soc.* **1953**, *36*, 207.
(23) Woodward, P. M. *Acta Crystallogr., Sect. B: Struct. Sci*. **1997**, *53*, 44.
(24) Shimizu, Y.; Shimalukuro, M.; Arai, H.; Seiyama, T. *J. Electrochem. Soc.* **1989**, *136*, 1206.
(25) Zhang, W. F.; Tang, J. W.; Ye, J. H. *Chem. Phys. Lett.* **2006**, *418*, 174.
(26) Zhang, W. F.; Tang, J. W.; Ye, J. H. *J. Mater. Res.* **2007**, *22*, 1859.
(27) Mizoguchi, H.; Eng, H. W.; Woodward, P. M. *Inorg. Chem.* **2004**, *43*, 1667.

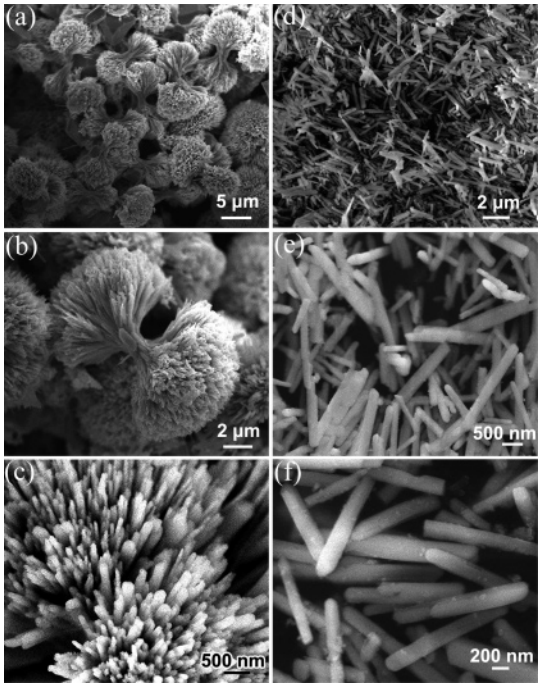

Figure 2. SEM images with different magnification of as-prepared precursor $SrSn(OH)_6$ dumbbells (a−c) and nanorods (d−f).

$SrSn(OH)_6$ Precursors. The FE-SEM images of the hydrothermally synthesized $SrSn(OH)_6$ precursors are shown in Figure 2. They clearly demonstrate the formation of two distinct products. One is the dumbbell-like product (Figure 2a−c); the other is the rodlike product (Figure 2d−f). The yields of products with dumbbell-like and rodlike morphology are very high as indicated in the low magnification images shown in both parts a and d of Figure 2, which also indicated that the samples with different morphologies prepared from the present process were with better reproducibility. Parts b and c of Figure 2 are the higher magnification SEM images of the synthesized dumbbell-like product. Each dumbbell consists of a large quantity of bundles of $SrSn(OH)_6$ nanorods, and they grow three-dimensionally from its center in uniform size-distribution of about 100−200 nm in diameters. Figure 2e,f shows the higher magnification SEM images of the rodlike $SrSn(OH)_6$ precursor, which consists of individual nanorods with diameters of about 200 nm and lengths of several microns.

Calcined $SrSnO_3$ Nanostructures. In the experiments, it was found that the products obtained after calcined at 1100 °C for 6 h still remain the morphology of the corresponding $SrSn(OH)_6$ precursors, as shown in Figure 3. Figure 3a gives a general SEM image of the calcined $SrSnO_3$ products obtained from the dumbbell-like $SrSn(OH)_6$ precursors, which still possesses the dumbbell-like morphology. The SEM images of an individual $SrSnO_3$ dumbbell are shown in Figure 3b,c. They clearly reveal that the obtained $SrSnO_3$ dumbbell still consists of a large quantity of homogeneous $SrSnO_3$ nanorods with diameters of about 150−200 nm and lengths up to several microns. TEM images shown in Figure 3e,f further conclude the dumbbell-like nanostructure is not a simple aggregation of small crystallites but is composed of rodlike monocrystallines growing homocentricly. The corresponding EDS spectrum of the dumbbell-like $SrSnO_3$ sample in Figure 3h shows that it is composed of Sr, Sn, and O atoms, and no other impurity was detected. In this spectrum, signals corresponding to Cu arise from the TEM grid. The high-resolution TEM (HRTEM) image of the $SrSnO_3$ product is shown in Figure 3d. The measured d spacings of about 0.4 nm correspond to the (002) and (110) planes of orthorhombic phase $SrSnO_3$. The selected area electron diffraction (SAED) pattern in Figure 3g indicates that the nanorod is single crystal and can be indexed as the $SrSnO_3$ orthorhombic phase, which is in accordance with the XRD result in Figure 1. The results confirm the formation of a single-crystalline $SrSnO_3$ nanorod with the preferred growth direction along the (001) orientations.

Figure 4a displays an overview SEM image of the $SrSnO_3$ nanorods obtained from the $SrSn(OH)_6$ nanorods precursor calcined at high temperature. It shows that randomly distributed nanorods obtained on a large scale possess the same shape with their corresponding $SrSn(OH)_6$ precursors. In fact, magnified SEM images in Figure 4b,c reveal that the morphology of $SrSnO_3$ nanorods was slightly destroyed after a heat-treatment process. The $SrSn(OH)_6$ nanorods have uniform diameters along the whole lengths, while the calcined $SrSnO_3$ nanorods have slightly wavy diameters due to the high-temperature calcinations effects. Figure 4e is a TEM image of the obtained $SrSnO_3$ nanorods, which further confirms that the surface of the nanorod was slightly destructive, and the diameter of a single nanorod is about 200 nm and the length is up to several microns. The corresponding EDS spectrum shown in Figure 4d shows the presence of Sr, Sn, and O elements, indicating the formation of $SrSnO_3$. The HRTEM image and the SAED pattern in Figure 4e,f also shows that the nanorod is of single-crytalline nature and grows along the (001) orientations.

Growth Process. Considering that there are no additional templates or surfactants in the present case, it is reasonable to presume that the growth and formation of nanostructures is not a catalyst-assisted or a template-assisted process since the only source materials used in this case are pure alkaline earth metal nitrate and metal stannate. A dissolution-recrystallization mechanism may be used to explain the formation of the corresponding nanostructures. At the first stage, the direct mixing of two solutions containing either Sr^{2+} or SnO_3^{2-} ions led to the formation of a large number of amorphous precursor particles at room temperature (about 25 °C), which is confirmed by the SEM image shown in Figure 5a. Then under hydrothermal conditions, with increasing temperature and pressure, these amorphous particles underwent a crystallization process, namely, amorphous precursor particles dissolved and the newly grown $SrSn(OH)_6$ nuclei formed. Later the bigger particles grew at the cost of the smaller ones, because there is different solubility between relatively larger and smaller particles according to the Gibbs−Thomson law.[28] Under this nonequilibrium kinetic growth condition, bigger rod-shaped particles appeared and tended to grow radically from the center. Finally, nearly dumbbell-like particles made of many rods formed after a

(28) Mullin, J. W. *Crystallization*, 3rd ed.; Butterworth-Heinemaan: Oxford, 1997.

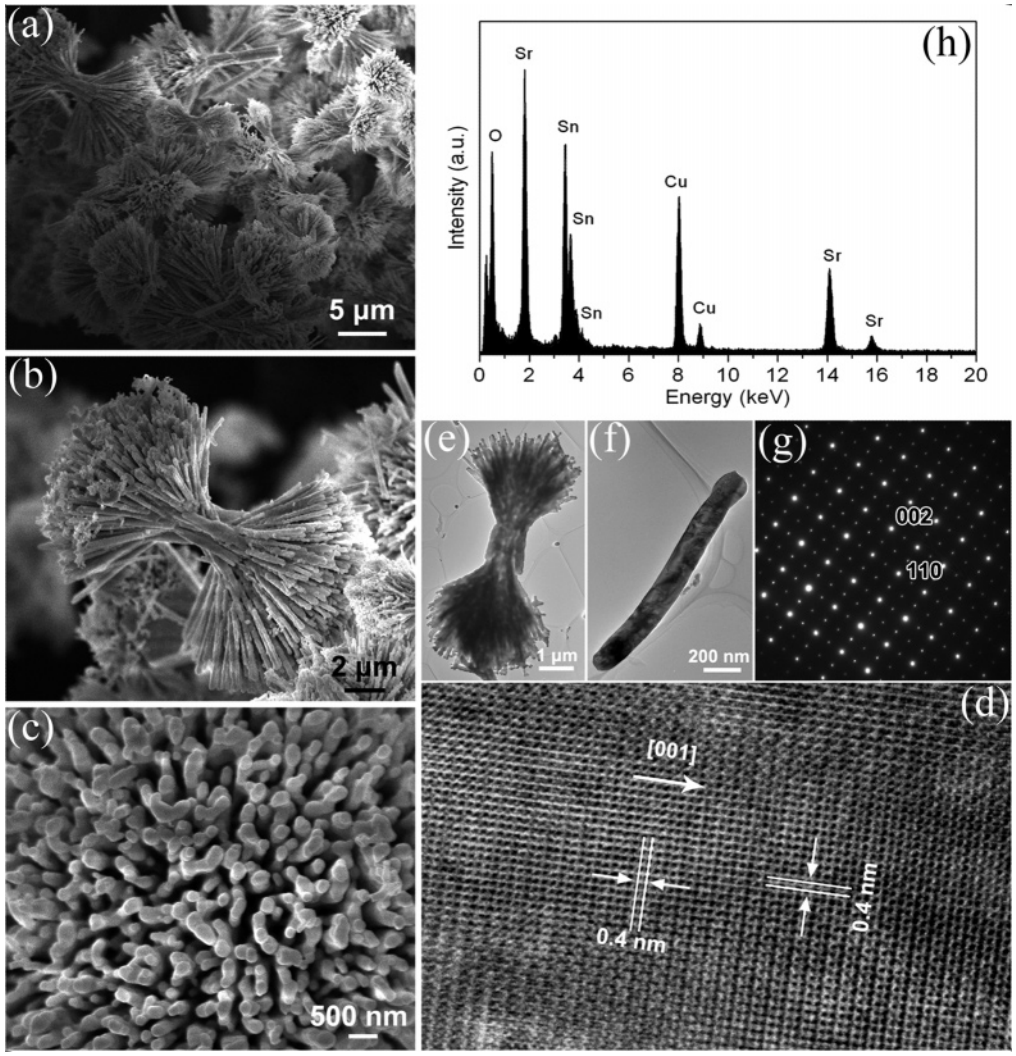

Figure 3. SEM images (a−c), TEM images (e, f), HRTEM image (d), SAED pattern (g), and EDS spectrum (h) of the dumbbell-like $SrSnO_3$ sample.

long time hydrothermal process. In the subsequent stage, reduction in surface energy is the primary driving force for crystal growth of the particles and morphology evolution. It is clear that the crystalline phase of the nuclei is critical for directing the intrinsic shape of the crystals due to its characteristic symmetry and structure. While the mixed solution was kept stirring for some time, in the present case, the stirring time is 2 h, and a rod-shaped precursor formed as shown in Figure 5b. Under the hydrothermal conditions, a rod-shaped precursor underwent a similar dissolution-recrystallization process, which resulted in the formation of $SrSn(OH)_6$ nanorods. In the present case, when raw material $Sr(NO_3)_2$ was substituted with $SrCO_3$, only bigger particulate precursors were obtained (see the Supporting Information, Figure S1), which indicated that the dissolvable metal salts used as raw materials is important for the morphologies of the final photocatalyst. Moreover, keeping the mixed solution stirred overnight at room temperature, somewhat, rodlike precursors were bigger and aggregated (see the Supporting Information, Figure S2). When the concentrations of reagents were increased, for example, 5 mmol of $Sr(NO_3)_2$ and Na_2SnO_3 was dissolved into 15 mL of distilled water to form solutions, respectively, and then two kinds of solutions were mixed at room temperature, and precursors with similar morphologies were obtained compared to those samples from the previous process. Based on the above experimental results, it can be seen that the dissolvable metal salts used as raw reagents and the stirring treatment play important roles on the morphology-controlling of the precursors which directly result in the morphology formation of final products. $SrSn(OH)_6$ was converted to $SrSnO_3$ during a subsequent calcination treatment process as a gradual elimination of water. Nevertheless, the conversion did not lead to any change in the morphology. The morphology was maintained perhaps because of the higher activation energy needed for the collapse of these structures.

Photocatalytic H_2 and O_2 Evolution Properties. Photocatalytic H_2 and O_2 evolution on the $SrSnO_3$ photocatalyst with different morphologies was performed under UV light irradiation, and the results were summarized in Table 1. Figure 6a presents the photocatalytic H_2 evolution with a Pt loaded cocatalyst from a methanol−water solution on the dumbbell-like and rodlike $SrSnO_3$ photocatalysts, respectively. It was clear that H_2 was evolved nearly linearly with irradiation time under the present experimental conditions except that the rodlike sample showed higher activity than the dumbbell-like sample. The average H_2 evolution rates were nearly 8.2 mmol/h·g for a rodlike photocatalyst and

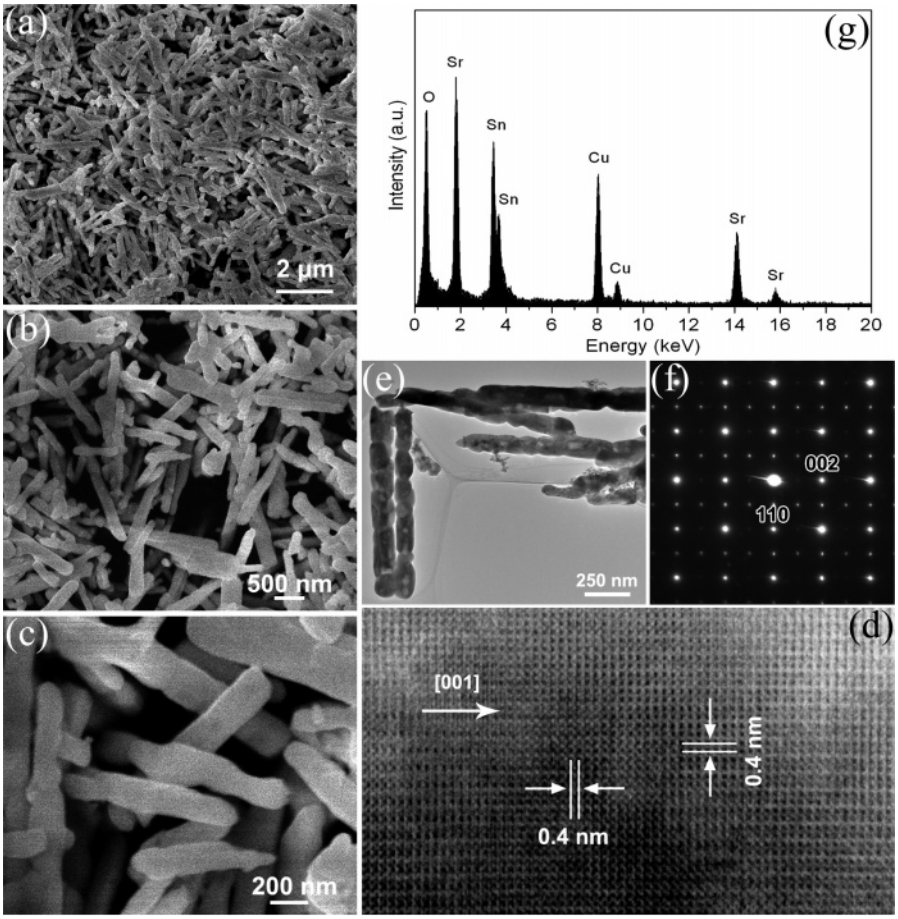

Figure 4. SEM images (a−c), TEM image (e), HRTEM image (d), SAED pattern (f), and EDS spectrum (g) of the nanorods $SrSnO_3$ sample.

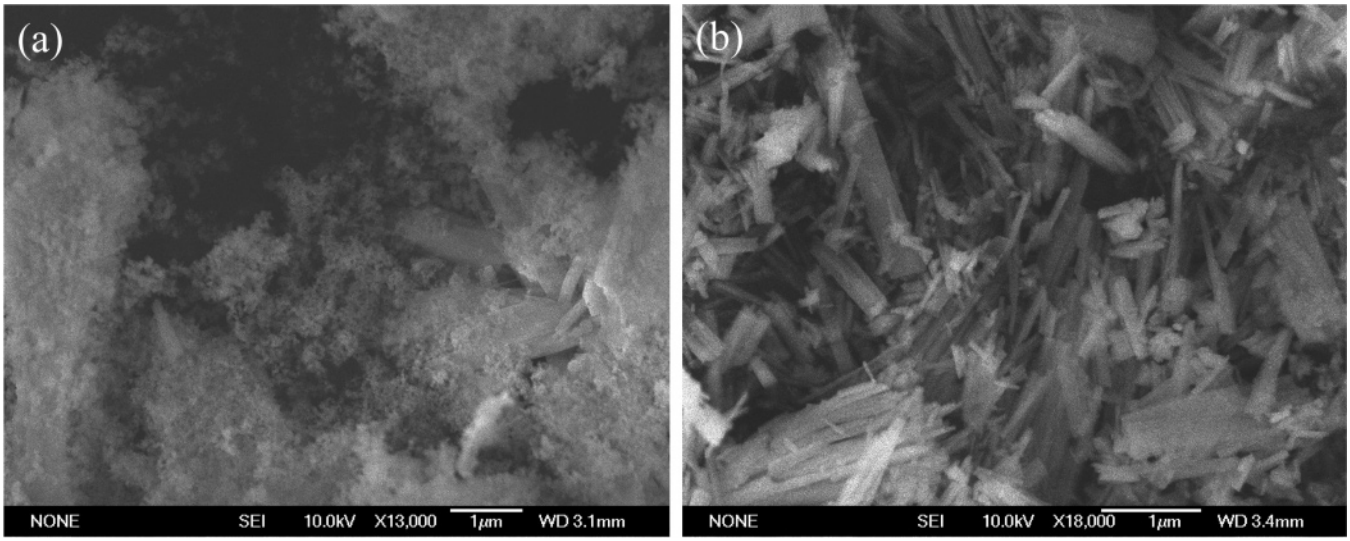

Figure 5. SEM images of (a) a particle precursor obtained after mixing the solution immediately and (b) a rodlike precursor obtained after stirring for 2 h.

7.2 mmol/h·g for a dumbbell-like photocatalyst, respectively. Figure 6b presents the photocatalytic O_2 evolution from the $AgNO_3$ aqueous solution on the samples with dumbbell-like and rodlike morphologies. The initial O_2 evolution rate of the rodlike photocatalyst (2.5 mmol/h·g) was slightly higher than that of the dumbbell-like photocatalyst (2.2 mmol/h·g). With increasing irradiation time, the O_2 evolution rates of two samples both decreased slightly, because the metallic Ag from the $AgNO_3$ sacrificial reagent shielded the incident light and reduced the surface active sites of the photocatalyst.[29,30] These results confirm that the $SrSnO_3$ nanorods exhibited superior photocatalytic activity compared to the dumbbell-like sample which might be due to the higher surface area of the rodlike sample favoring the photocatalytic reaction at the surface. The photonic efficiency of the Pt-loaded $SrSnO_3$ dumbbell-like photocatalyst at 300 nm under 200 W Hg−Xe lamp irradiation amounted to 4.6%. In

(29) Kudo, A.; Omori, K.; Kato, H. *J. Am. Chem. Soc.* **1999**, *121*, 11459.
(30) Tang, J.; Zou, Z.; Ye, J. *J. Phys. Chem. B* **2003**, *107*, 14265.

Table 1. Photocatalytic Activity and Physical Properties of $SrSnO_3$ Photocatalyst

morphology	cryst struct	band gap[a] (eV)	BET (m^2/g)	rate of H_2 evolution[b] (mmol/h·g)	rate of O_2 evolution[c] (mmol/h·g)
dumbbell	orthorhombic	4.1	0.4	7.2	2.2
nanorod	orthorhombic	4.1	0.5	8.2	2.5
particle[d]	orthorhombic	4.1	0.3	0.72	0.28

[a] Estimated from the onset of absorption. [b] Catalyst: 0.2 g, Pt: 0.5 wt %, 50 mL of CH_3OH/320 mL of H_2O, light: 400 W high-pressure Hg lamp. [c] Catalyst: 0.2 g, $AgNO_3$: 0.85 g, 370 mL of H_2O, light: 400 W high-pressure Hg lamp. [d] Dr Zhang's results from solid-state route:[25,26] H_2 evolution: catalyst: 0.5 g, Pt 0.5 wt %, 50 mL of CH_3OH/320 mL of H_2O, light: 400 W high-pressure Hg lamp. O_2 evolution: catalyst: 0.5 g, $AgNO_3$: 0.85 g, 370 mL of H_2O, light: 400 W high-pressure Hg lamp.

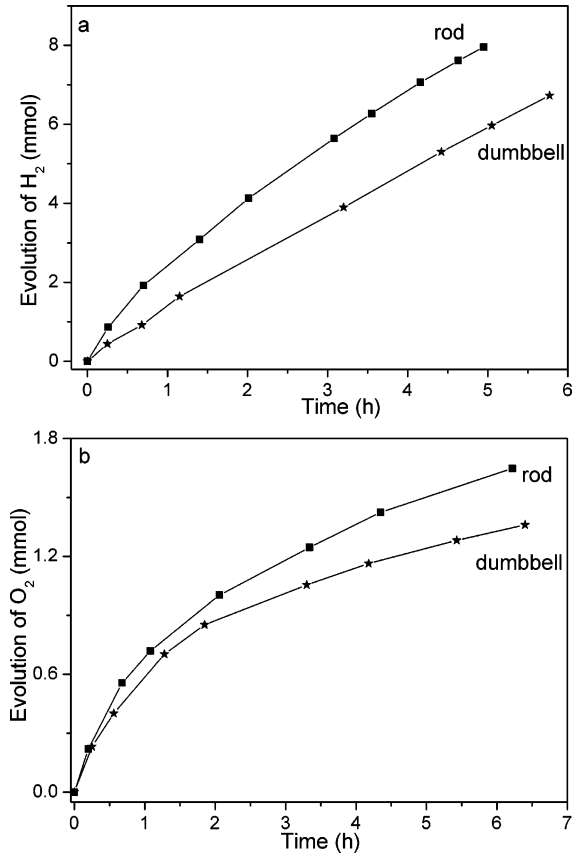

Figure 6. (a) Photocatalytic H_2 evolution from the aqueous solution of methanol and (b) O_2 evolution from the aqueous silver nitrate solution, respectively, under UV light irradiation over the dumbbell-like and nanorodlike $SrSnO_3$ photocatalysts, respectively.

addition, as shown in Table 1, samples obtained from the present route exhibited much higher photoactivity for the H_2 and O_2 evolution under UV light irradiation than the SSR sample.[25,26] In our experiment results, the sample from the solid-state route was aggregated particles, and the surface area was 0.3 m^2/g (see the Supporting Information, Figure S3). It is well-known that samples from the hydrothermal process usually possess smaller crystallite size and lower agglomeration, which led to the high photocatalytic activity under light irradiation.

Furthermore, the photocatalytic H_2 evolution without a Pt loaded cocatalyst from a methanol−water solution on the dumbbell-like photocatalyst was studied, and the rate of H_2 evolution was about 0.02 mmol/h·g in the first 1 h of the

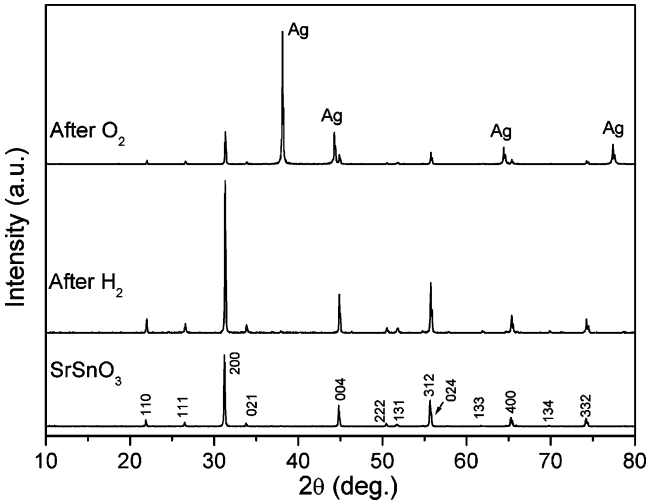

Figure 7. XRD patterns of the $SrSnO_3$ before and after photocatalytic H_2 and O_2 evolution.

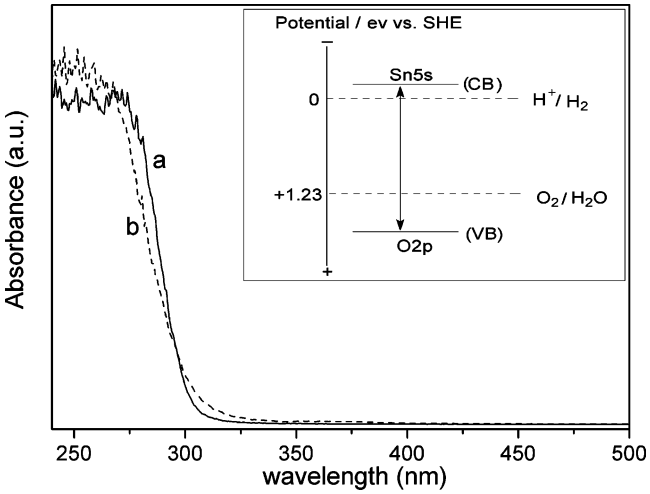

Figure 8. UV−vis diffuse reflectance spectra of $SrSnO_3$ with nanorodlike (dot line) and dumbbell-like (solid line) morphology. The inset is the suggested diagram of the band structure of $SrSnO_3$, VB is the valence band, and CB is the conduction band.

reaction (see the Supporting Information, Figure S4). In general, a loading noble metal, such as Pt, as a cocatalyst on the surface of a semiconductor can be effective in changing the semiconductor surface properties by increasing active sites and suppressing charge recombination thus enhancing photocatalytic activity. The stability of the photocatalyst was further confirmed by the XRD results. Figure 7 shows the XRD patterns of the $SrSnO_3$ photocatalyst before and after the photocatalytic H_2 and O_2 evolution. It can be seen that the XRD patterns of the photocatalyst after the H_2 and O_2 evolution reaction did not change except that several new metallic Ag peaks appear during the photocatalytic O_2 evolution, suggesting that the sample is stable for photocatalytic water splitting. The UV−visible diffuse reflectance spectra of dumbbell-like and nanorodlike photocatalysts are shown in Figure 8. It can be seen that dumbbell-like and nanorodlike $SrSnO_3$ samples showed strong absorption in the UV light region. Both of these samples present almost the same onset of absorption around 300 nm, and the estimated band gap was 4.1 eV. The inset shows the suggested band structure of $SrSnO_3$ photocatalyst. Based on the previous experimental results,[25,26] the photogenerated

electron transfers from the O 2p orbital to the Sn 5s orbital under UV light irradiation. The CB and VB potential levels meet the potential requirements of H_2 and O_2 evolution, namely, the bottom of the CB is more negative than the potential level of H^+/H_2 and the top of the VB is more positive than that of O_2/H_2O. And so H_2 and O_2 evolution under UV light irradiation is reasonable.

The photoactivities of the samples calcined at different temperature were also investigated by using the photocatalytic H_2 evolution as a model reaction, and the results showed that the calcinations-temperature has a significant effect on the photoactivities of the as-synthesized samples. When the sample was calcined at 650−1000 °C, almost no H_2 evolution was detected after several hours of work with constant UV light irradiation. A corresponding XRD result confirmed that sample calcined at lower temperature was with low crystallinity and was unstable after UV light irradiation because some weak peaks of impurities appeared in the patterns which can be indexed to orthorhombic Sr_2SnO_4. While the sample was calcined at higher temperature, such as 1200 °C, which also exhibited much lower activity for H_2 evolution, compared to the sample calcined at 1100 °C. The UV diffuse reflectance spectrum of $SrSnO_3$ sample obtained at 1200 °C displayed a weak and broad absorption at about 530 nm, which can be attributed to the defects level. It is well-known that lattice defects may act as recombination centers for the photoinduced electrons and holes, thus significantly reducing the net photocatalytic activity.[31,32] The decrease in the photocatalytic activity when the sample is calcined at higher temperature may therefore be understood in such a way, namely, that lattice defects acting as inactivation centers are increased due to the overheated treatment process. In this work, the color of the sample changed from white to red after calcined at 1200 °C for 6 h which also illuminated the existence of defects and the decrease of the photocatalytic activity of the sample.

4. Conclusion

In summary, $SrSn(OH)_6$ and $SrSnO_3$ nanostructures with dumbbell-like and rodlike morphologies have been successfully achieved by a facile hydrothermal process and subsequent heat-treatment process, respectively. The shape and size of $SrSn(OH)_6$ and $SrSnO_3$ can be modulated by the stirring treatment. The as-prepared $SrSnO_3$ nanostructures showed higher activity for H_2 and O_2 evolution than the sample from the solid-state route under UV light irradiation. These results highlight that the shape-controlled synthesis of material with favorable photocatalytic property is a promising strategy to develop highly efficient photocatalytic materials.

Acknowledgment. This work was partially supported by the Global Environment Research Fund from the Ministry of Education, Culture, Sports, Science and Technology (MEXT) of the Japanese Government. The authors are also grateful to Ms. Liqun Yang for help with the experiment.

Supporting Information Available: SEM image of the precursor obtained from mixing $SrCO_3$ and Na_2SnO_3 solutions at room temperature, SEM image of the precursor obtained after the mixed solution system was stirred overnight at room temperature, SEM images of the sample from the solid-state route, and photocatalytic H_2 evolution from the aqueous solution of methanol under UV light irradiation over the dumbbell-like $SrSnO_3$ photocatalyst without a Pt cocatalyst. This material is available for free of charge via the Internet at http://pubs.acs.org.

CM071321D

(31) Yoshino, M.; Kakihana, M. *Chem. Mater.* **2002**, *14*, 3369.
(32) Zou, Z.; Ye, J.; Arakawa, H. *J. Phys. Chem. B* **2002**, *106*, 517.